Inorg. Chem. **2007**, *46*, 7935–7943

Synthesis, Structure, and Upconversion Studies on Organically Templated Uranium Phosphites

Sukhendu Mandal,[†] Manabendra Chandra,[‡] and Srinivasan Natarajan*,[†]

Framework Solids Laboratory, Solid State and Structural Chemistry Unit, Indian Institute of Science, Bangalore 560012, India and the Department of Inorganic and Physical Chemistry, Indian Institute of Science, Bangalore 560012, India

Received May 5, 2007

Three new amine templated uranium phosphites, $[C_2N_2H_{10}][U_2^{IV}F_6(HPO_3)_2]$, **1**, $[C_4N_2H_{12}][U_2^{IV}F_6(HPO_3)_2]$, **2**, and $[C_4N_2H_{12}][(U^{VI}O_2)_2F_2(HPO_3)_2]$, **3**, have been synthesized by hydrothermal methods. All of the compounds are built up from a connectivity between $U(O/F)_x$ ($x = 7$, 8) and HPO_3 polyhedral units. The observation of a well-established secondary building unit, SBU-4, in **1** and **2** is noteworthy. In **1**, the SBU-4 units are connected to form U–F–U chains, which are linked by U–O–P chains, forming the layered structure. In **2**, the SBU-4 units are edge-shared and also interconnected forming the 3D structure. In **3**, the connectivity between the building units forms a layer, the topology of which is similar to the mineral, johannite. To the best of our knowledge, this is the first observation of a well-known secondary building unit (SBU-4) in actinide framework compounds. Optical studies on **1** and **2**, containing U^{4+} species, indicate an intense blue emission through an upconversion process, and the magnetic susceptibility studies show antiferromagnetic behavior.

Introduction

There is currently much interest in the study of compounds exhibiting open structures based on phosphite networks. The phosphite compounds, like the phosphate-based ones, show excellent variety and diversity in their structures.[1] Intense research activity during the past few years resulted in the isolation of many phosphites, for example, Zn,[2] V[3], Cr,[4] Mn,[5] Fe,[6] Co,[7] etc. Whereas a large number of organically templated transition and main-group element phosphites have been synthesized, research on lanthanide and actinide phosphites has been rare.[8] Uranium-based compounds are being investigated because of their remarkable coordination chemistry, relevance to geochemistry, and possible applications in the area of ion-exchange, catalysis, etc.[9] Most of the reported open-framework phosphate and phosphite com-

* To whom correspondence should be addressed. E-mail: snatarajan@sscu.iisc.ernet.in.

[†] Framework Solids Laboratory.

[‡] Department of Inorganic and Physical Chemistry.

(1) Maspoch, D.; Ruiz-Molina, D.; Veciana, J. *Chem. Soc. Rev.* **2007**, *37*, 770.

(2) (a) Linag, J.; Li, J.; Yu, J.; Chen, P.; Fang, Q.; Sun, F.; Xu, R. *Angew. Chem., Int. Ed.* **2006**, *45*, 2546. (b) Chen, L.; Bu, X. *Inorg. Chem.* **2006**, *45*, 4654.

(3) (a) Shi, Z.; Li, G.; Zhang, D.; Hua, J.; Feng, S. *Inorg. Chem.* **2003**, *42*, 2357. (b) Fu, W.; Liang, G.; Sun, Y. *Polyhedron* **2006**, *25*, 2571.

(4) (a) Fernandez, S.; Mesa, J. L.; Pizarro, J. L.; Lezama, L.; Arriortua, M. I.; Rojo, T. *Chem. Mater.* **2003**, *15*, 1204. (b) Fernandez, S.; Mesa, J. L.; Pizarro, J. L.; Lezama, L.; Arriortua, M. I.; Rojo, T. *Angew. Chem., Int. Ed.* **2002**, *41*, 3683.

(5) Fernandez, S.; Mesa, J. L.; Pizarro, J. L.; Lezama, L.; Arriortua, M. I.; Olazcuaga, Rojo, R., T. *Chem. Mater.* **2000**, *12*, 2092.

(6) (a) Mandal, S.; Pati, S. K.; Green, M. A.; Natarajan, S. *Chem. Mater.* **2005**, *17*, 638. (b) Chung, U-C.; Mesa, J. L.; Pizarro, J. L.; Rodriguez, F. J.; Sancez, M. J.; Garitaonadia, J. S.; Arriortua, M. I.; Rojo, T. *Inorg. Chem.* **2006**, *45*, 8965.

(7) Fernandez, S.; Pizarro, J. L.; Mesa, J. L.; Lezama, L.; Arriortua, M. I.; Rojo, T. *Int. J. Inorg. Mater.* **2001**, *3*, 331.

(8) (a) Doran, M.; Walker, S. M.; O'Hare, D. *Chem. Commun.* **2001**, 1988. (b) Jian-F, X.; Hao-Hong, L.; Yan-Ning, C.; Chang-Cang, H.; Han-Hui, Z.; Dong-Sheng, L.; Qi-Yu, Y.; Rui-Qing, S. *J. Struct. Chem.* **2006**, *25*, 1380.

(9) (a) Almond, P. M.; Deakin, L.; Mar, A.; Albrecht-Schmitt, T. E. *Inorg. Chem.* **2001**, *40*, 886. (b) Danis, J. A.; Runde, W. H.; Scott, B.; Fettinger, J.; Eichhorn, B. *Chem. Commun.* **2001**, 2378. (c) Francis, R. J.; Halasyamani, P. S.; O'Hare, D. *Angew. Chem., Int. Ed.* **1998**, *37*, 2214. (d) Norquist, A. J.; Thomas, P. M.; Doran, M. B.; O'Hare, D. *Chem. Mater.* **2002**, *14*, 5179. (e) Wang, X.; Huang, J.; Jacobson, A. J. *J. Am. Chem. Soc.* **2002**, *124*, 15190. (f) Almond, P. M.; Deakin, L.; Porter, M. J.; Mar, A.; Albrecht-Schmit, T. E. *Chem. Mater.* **2000**, *12*, 3208. (g) Francis, R. J.; Halasyamani, P. S.; O'Hare, D. *Chem. Mater.* **1998**, *10*, 3131. (h) Francis, R. J.; Halasyamani, P. S.; Bee, J. S.; O'Hare, D. *J. Am. Chem. Soc.* **1999**, *121*, 1609. (i) Almond, P. M.; Deakin, A. M.; Albrecht-Schmitt, T. E. *Inorg. Chem.* **2001**, *158*, 87. (j) Cahill, C. L.; Burns, P. C. *Inorg. Chem.* **2001**, *40*, 1347. (k) Allen, S.; Barlow, S.; Halasyamani, P. S.; Mosselmans, J. F. W.; O'Hare, D.; Walker, S. M.; Walton, R. I. *Inorg. Chem.* **2000**, *39*, 3791. (l) Almond, P. M.; Ralley, C. E.; Bean, A. C.; Peper, S. M.; Albrecht-Schmitt, T. E. *J. Solid State Chem.* **2000**, *154*, 635. (m) Wang, C-M.; Liao, C-H.; Lin, H-M.; Lii, K-H. *Inorg. Chem.* **2004**, *43*, 8239. (n) Almond, P. M.; Deakin, L.; Mar, A.; Albrecht-Schmitt, T. E. *J. Solid State Chem.* **2001**, *158*, 87.

10.1021/ic700866f CCC: $37.00
Published on Web 08/24/2007

pounds of uranium possess uranium in a +6 oxidaton state.[10,8] The synthesis of three-dimensionally extended structures based on uranium is a great challenge. We have been interested in the study of uranium phosphites to understand the reactivity, the coordination preferences, and the oxidation state of uranium. During the course of this study, we have now prepared three new uranium phosphites. The compounds, $[C_2N_2H_{10}][U_2^{IV}F_6(HPO_3)_2]$, **1,** $[C_4N_2H_{12}][U_2^{IV}F_6(HPO_3)_2]$, **2**, and $[C_4N_2H_{12}][(U^{VI}O_2)_2F_2(HPO_3)_2]$, **3**, have been prepared, employing hydrothermal methods. Of these, **1** and **2** have uranium in a +4 oxidation state. In this article, we describe the synthesis, structure, optical, and magnetic properties.

Experimental Section

The uranium phosphites **1**, **2**, and **3** were synthesized using hydrothermal methods. Typically, for the synthesis of **1,** $UO_2(OAc)_2{\cdot}2H_2O$ (1.0603 g) was dispersed in 9 mL of water. To this, H_3PO_3 (0.82 g) and ethylenediamine (*en*) (0.16 mL) were added with constant stirring. Finally, HF (48%, 0.35 mL) was added, and the mixture was homogenized at room temperature. The final reaction mixture with the composition $1UO_2(OAc)_2{\cdot}2H_2O/4H_3PO_3/1$*en*$/4HF/200H_2O$ was heated in a 23 mL PTFE-lined stainless steel acid-digestion vessel at 180 °C for 24 h, followed by heating at 200 °C for 24 h. For the synthesis of **2**, $UO_2(OAc)_2{\cdot}2H_2O$ (1.0603 g) was dispersed in 9 mL of water. To this, H_3PO_3 (0.82 g) and piperazine (PIP) (0.21 g) were added with constant stirring. Finally, HF (48%, 0.35 mL) was added, and the mixture was homogenized at room temperature. The final reaction mixture with the composition $1UO_2(OAc)_2{\cdot}2H_2O/4H_3PO_3/1PIP/4HF/200H_2O$ was heated in a 23 mL PTFE-lined stainless steel acid-digestion vessel at 180 °C for 24 h, followed by heating at 200 °C for 24 h. For the preparation of **3**, a reaction composition of $1UO_2(OAc)_2{\cdot}2H_2O/4H_3PO_3/1$[1-(2-aminoethyl) piperazine (AEPIP)]$/4HF/200H_2O$ was heated at 180 °C for 24 h, followed by heating at 200 °C for 24 h. The resulting product in each of the cases contained good quality single crystals suitable for single-crystal X-ray diffraction, which were filtered and washed thoroughly with deionized water. Thus, green plate-like (**1**), green rod-like (**2**), and yellow plate-like (**3**) crystals were obtained with good yields (65% for **1**, 70% for **2**, and 80% for **3**; based on uranium).

Initial characterizations were carried out by elemental analysis, energy dispersive X-ray analysis (EDAX), powder X-ray diffraction (XRD), thermogravimetric analysis (TGA), and IR spectroscopic studies. Elemental analysis of the crystals was carried out using atomic absorption spectroscopy (ThermoFinnigan FLASH EA 1112 CHNS analyzer). Elemental Anal. Calcd for **1**: C 2.95, H 1.49, N 3.44; found: C 2.40, H 1.16, N 3.16; Calcd for **2**: C 5.57, H 1.68, N 3.34; found: C 5.08, H 1.82, N 3.04; Calcd for **3**: C 5.81, H 1.70, N 3.39; found: C 5.28, H 1.85, N 3.02. An EDAX analysis on many single crystals indicated a ratio of uranium: $P = 1{:}1$ for all of the compounds, in addition to the presence of fluorine.

The powder XRD patterns were recorded on crushed single crystals in the 2θ range 5−50°, using Cu Kα radiation (Philips X'pert Pro). The XRD patterns of the compounds were entirely consistent with the simulated XRD patterns obtained from the structures determined using single-crystal XRD (Supporting information, Figures S1, S2, and S3).

TGA (Mettler−Toledo, ThermoSTAR) studies were performed in an atmosphere of flowing air (flow rate = 50 mL/min) in the temperature range 25−800 °C (heating rate = 5 °C/min). The result indicated a two-step weight loss for all of the compounds (Supporting information, Figure S4). The first weight loss in the region 250−450 °C corresponds to the decomposition of amine molecules, and the second weight loss in the range 450−750 °C corresponds to the loss of fluorine. It is likely that the water molecules formed during the combustion of the organic molecule hydrolyze the fluoride ion in the framework, thereby resulting in the formation of volatile hydrogen fluoride. The calculated weight loss total for the amine and the fluorine molecules are 21.67% (7.64 + 14.03) for **1** and 24.11% (10.51 + 13.60) for **2**. The observed weight losses are 14.86% for **1** and 21.66% for **2**. These differences between the calculated and observed weight loss can be explained by considering the oxidation of P(III) to P(V) and U(IV) to U(VI) for all of the compounds. The calculated weight gain due to the oxidation of P(III) to P(V) is 3.94% for **1** and 3.81% for **2**, respectively. For **1** and **2**, the calculated weight gain due to the oxidation of U(IV) to U(VI) is 1.97 and 1.90%, respectively. Thus, the total weight loss would be 20.77% (14.86 + 3.94 + 1.97) for **1** and 27.37% (21.66 + 3.81 + 1.90) for **2**, which is much closer to the calculated weight loss of 21.67% for **1** and 24.22% for **2**, respectively.

IR spectroscopic studies were carried out in the range of 300−4000 cm^{-1}, using the KBr pellet method (Perkin-Elmer, SPECTRUM 1000). IR spectroscopic studies exhibited typical peaks corresponding to the amine molecule, the metal−fluorine bond, and the HPO_3 moiety for all of the compounds, with little variations in their respective bands (Supporting information, Figure S5). IR (KBr): $\nu_s(N-H) = 3110-3390\ cm^{-1}$, $\nu_s(C-H)_{asym} = 2850-3050\ cm^{-1}$, $\nu_s(C-H)_{sym} = 2825-2990\ cm^{-1}$, $\nu_s(P-H) = 2402-2427\ cm^{-1}$, $\delta_s(N-H) = 1515-1620\ cm^{-1}$, $\delta_s(C-H) = 1450-1480\ cm^{-1}$, $\nu_s(C-N) = 1090-1130\ cm^{-1}$, $\nu_{as}(P-O) = 1050-1080\ cm^{-1}$, $\delta_{as}(P-H) = 950-1020\ cm^{-1}$, $\nu_s(P-O) = 820-920\ cm^{-1}$, $\delta_s(P-O) = 550-600\ cm^{-1}$, $\delta_{as}(P-O) = 450-533\ cm^{-1}$, $\nu_s(U-F) = 360-390\ cm^{-1}$.

Single-Crystal Structure Determination. A suitable single crystal of each compound was carefully selected and glued to a thin glass fiber. The single-crystal X-ray diffraction data were collected on a Bruker AXS Smart Apex CCD diffractometer at 293(2) K. The X-ray generator was operated at 50 kV and 35 mA using Mo Kα ($\lambda = 0.71073$ Å) radiation. Data were collected with ω scans of width 0.3°. A total of 606 frames were collected in three different settings of φ (0°, 90°, 180°) keeping the sample-to-detector distance fixed at 6.03 cm and the detector position (2θ) fixed at −25°. Pertinent experimental details of the structure determination of all of the compounds are presented in Table 1.

The data were reduced using *SAINTPLUS*,[11] and an empirical absorption correction was applied using the *SADABS* program.[12] The crystal structure was solved and refined using *SHELX-97*[13] present in the *WinGx* suit of the program (Ver. 1.63.04a). The hydrogen atom on the P−H group and the hydrogen positions of the amine molecules of all of the compounds were located in the difference Fourier map, and for the final refinement, the hydrogen

(10) (a) Francis, R. J.; Drewitt, M. J.; Halasamani, P. S.; Ranganathachar, C; O'Hare, D.; Clegg, W.; Teat, S. J. *Chem. Commun.* **1998**, 279. (b) Danis, J. A.; Runde, W. H.; Scott, B.; Fettinger, J.; Eichhorn, B. *Chem. Commun.* **2001**, 2378. (c) Doran, M. B.; Stuart, C. L.; Norquist, A. J.; O'Hare, D. *Chem. Mater.* **2004**, *16*, 565. (d) Ok, K. M.; Baek, J.; Halasyamani, P. S.; O'Hare, D. *Inorg. Chem.* **2006**, *45*, 10270. (e) Locock, A. J.; Burns, P. C. *J. Solid State Chem.* **2004**, *17*, 2675.

(11) *SMART* (ver. 5.628), *SAINT* (ver. 6.45a), *XPREP*, *SHELXTL*; Bruker AXS Inc.: Madison, WI, 2004.

(12) Sheldrick, G. M. *Siemens Area Correction Absorption Correction Program*; Universuty of Göttingen: Göttingen, Germany, 1994.

(13) Sheldrick, G. M. *SHELXL-97 Program for Crystal Structure Solution and Refinement*; University of Göttingen: Göttingen, Germany, 1997.

Table 1. Crystal Data and Structure Refinement Parameters for $[C_2N_2H_{10}][U_2^{IV}F_6(HPO_3)_2]$, **1**, $[C_4N_2H_{12}][U_2^{IV}F_6(HPO_3)_2]$, **2**, and $[C_4N_2H_{12}][(U^{VI}O_2)_2F_2(HPO_3)_2]$, **3**

compound	**1**	**2**	**3**
empirical formula	$C_1H_6N_1O_3F_3P_1U_1$	$C_2H_7N_1O_3F_3P_1U_1$	$C_2H_7N_1O_5F_1P_1U_1$
cryst syst	triclinic	monoclinic	triclinic
space group	$P(\bar{1})$	$P2_1/c$	$P(\bar{1})$
cryst size (mm)	0.20 × 0.10 × 0.08	0.16 × 0.10 × 0.08	0.18 × 0.10 × 0.08
a (Å)	6.1929(18)	7.338(2)	6.725(2)
b (Å)	7.225(2)	10.669(3)	6.901(2)
c (Å)	7.999(2)	9.383(3)	9.272(3)
α (deg)	92.453(4)	90.00	103.186(4)
β (deg)	102.094(4)	102.581(4)	111.028(4)
γ (deg)	108.916(4)	90.00	97.386(4)
V (Å^3)	328.68(17)	716.9(3)	380.4
Z	2	4	2
ρ (g cm^{-3})	4.103	3.883	3.606
μ (mm^{-1})	24.946	22.881	21.540
λ (Å)	0.71073	0.71073	0.71073
θ range (deg)	3.00−27.03	2.93−26.37	2.46−25.35
reflns collected	3026	4802	3504
unique reflns	1281	1309	1341
GOF	1.084	1.031	1.083
R index [$I > 2\sigma(I)$]	R1 = 0.0318, wR2 = 0.0821	R1 = 0.0376, wR2 = 0.0983	R1 = 0.0349, wR2 = 0.0976
R, all data[a]	R1 = 0.0322, wR2 = 0.0824	R1 = 0.0407, wR2 = 0.1013	R1 = 0.0356, wR2 = 0.0981

[a] $R1 = \sum||F_o| - |F_c||/\sum|F_o|$; $wR2 = \{\sum[w(F_o^2 - F_c^2)]/\sum[w(F_o^2)^2]\}^{1/2}$. $w = 1/[\rho^2(F_o)^2 + (aP)^2 + bP]$. $P = [\max(F_o, O) + 2(F_c)^2]/3$, where $a = 0.0433$ and $b = 2.4483$ for **1**, $a = 0.0704$ and $b = 4.8040$ for **2**, and $a = 0.0523$ and $b = 6.2015$ for **3.**

atoms were placed in geometrically ideal positions and refined using the riding mode. The last cycles of refinements included atomic positions, anisotropic thermal parameters for all of the non-hydrogen atoms, and isotropic thermal parameters for all of the hydrogen atoms. Full-matrix least-squares structure refinement against $|F|^2$ was carried out using the *WINGX*[14] package of programs. CCDC Nos. 645790−645791 for compounds **1**, **2**, and 645789 for **3** contain the crystallographic information for this article. These data can be obtained free of charge from The Cambridge Crystallographic Data Center (CCDC) via www.ccdc.cam.ac.uk/data_request/cif.

Results

$[C_2N_2H_{10}][U_2^{IV}F_6(HPO_3)_2]$, 1. The asymmetric unit of $[C_2N_2H_{10}][U_2^{IV}F_6(HPO_3)_2]$, **1**, contains 10 non-hydrogen atoms, of which one uranium and one phosphorus atom are crystallographically independent (Supporting Information). The uranium atom is bonded to three oxygen and five fluorine atoms, forming a distorted dodecahedral geometry (part a of Figure 1). Of the five fluorine atoms, four bridge the uranium centers, and the remaining one is terminal. The U−F bond distances are in the range of 2.182(5)−2.421(5) Å (average 2.330 Å), the shorter distances corresponding to the terminal U−F bond. The U−O bond distances are in the range of 2.182(5)−2.324(7) Å (average 2.300 Å). The O/F−U−O/F bond angles are in the range of 65.2(2)−145.1(2)°. The phosphorus atom has three P−O−U bonds. The P−O bond distances are in the range 1.511(7)−1.527(7) Å (average 1.518 Å). The bond valence sum calculations indicate the valence state of uranium to be +4 ($\sum$s(U− O/F) = 3.96).[15] Selected bond distances are given in Table 2.

The structure of **1** consists of a network of UO_3F_5 and HPO_3 units. The UO_3F_5 units are connected edge-wise

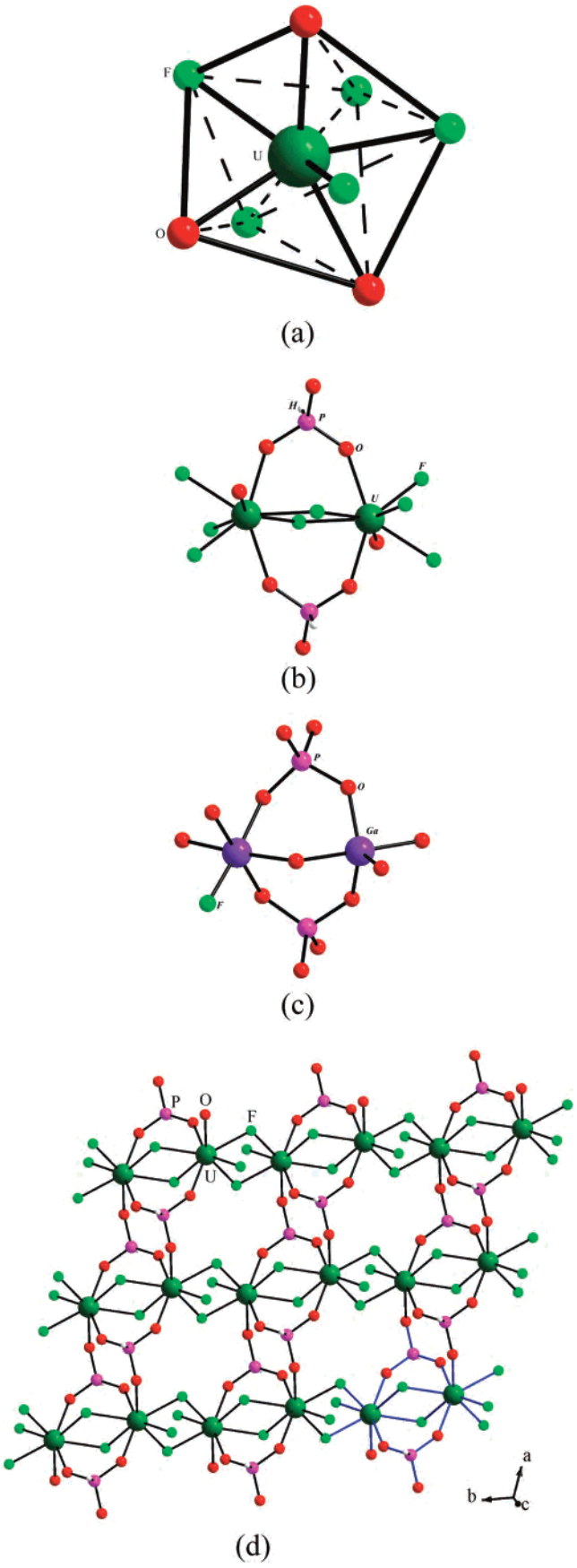

Figure 1. (a) Coordination geometry around U^{4+} ions in $[C_2N_2H_{10}][U_2^{IV}F_6(HPO_3)_2]$, **1.** (b) SBU-4 unit in **1**. (c) SBU-4 unit in $(NH_4)_{0.53}(H_3O)_{0.07}[GaPO_4(OH)_{0.5}F_{0.5}]$.[16d] Note the close similarity between the two SBUs. (d) Ball−stick view of the layer, showing the infinite U−F−U bond (text).

(14) Farrugia, J. L. *J. Appl. Crystallogr.* **1999**, *32*, 837−838.

Table 2. Selected Bond Lengths in $[C_2N_2H_{10}][U_2^{IV}F_6(HPO_3)_2]$, **1**, and $[C_4N_2H_{12}][U_2^{IV}F_6(HPO_3)_2]$, **2**[a]

bond	distance (Å)	bond	distance (Å)
Compound **1**			
U(1)−O(1)	2.279(6)	U(1)−F(3)#1	2.369(5)
U(1)−O(2)	2.298(7)	U(1)−F(2)#2	2.421(5)
U(1)−O(3)	2.324(7)	P(1)−O(1)#3	1.511(7)
U(1)−F(1)	2.182(5)	P(1)−O(2)	1.527(7)
U(1)−F(2)	2.314(5)	P(1)−O(3)#1	1.517(7)
U(1)−F(3)	2.367(5)		
Compound **2**			
U(1)−O(1)	2.266(6)	U(1)−F(3)#1	2.422(5)
U(1)−O(2)	2.359(5)	U(1)−F(2)#2	2.451(5)
U(1)−O(3)	2.335(5)	P(1)−O(1)#3	1.541(6)
U(1)−F(1)	2.178(4)	P(1)−O(2)#1	1.529(6)
U(1)−F(2)	2.285(4)	P(1)−O(3)	1.521(6)
U(1)−F(3)	2.340(4)		

[a] Symmetry transformations used to generate equivalent atoms: For **1**: #1 $-x+1, -y+2, -z+1$; #2 $-x+1, -y+1, -z+1$; #3 $-x+2, -y+2, -z+1$. For **2**: #1 $-x+1, -y+2, -z+2$; #2 $-x+2, -y+2, -z+2$; #3 $-x+1, y-{}^1/_2, -z+{}^3/_2$.

through the fluorine atoms forming the dimer, $U_2O_6F_8$, which are capped on either side by HPO_3 units, forming the basic secondary building unit (part b of Figure 1), which closely resembles one of the secondary building units, SBU-4, proposed by Ferey (part c of Figure 1).[16] The SBU-4 units have been first observed in the gallium phosphate, $(NH_4)_{0.93}(H_3O)_{0.07}[GaPO_4(OH)_{0.5}F_{0.5}]$.[16d] Though the SBU-4 units identified in the present compound differ from those observed in the gallium phosphate, similar edge-shared SBU-4 units have been observed in many other compounds.[16f] The SBU-4 units are connected to form the layered structure with infinite 1D U−F−U chains. The entire structure can be explained on the basis of SBU-4 units, where in one direction they are connected through fluorine bridges (U−F−U) and in the other direction through U−O−P linkages (part d of Figure 1). The ethylenediamine molecules occupy the interlayer spaces and interact with the framework through N−H···F hydrogen bond interactions, [N(1)−H(3)···F(1) (N−F = 2.832 Å, N(1)−H(3)···F(1) = 152°].

$[C_4N_2H_{12}][U_2^{IV}F_6(HPO_3)_2]$, 2. The asymmetric unit of $[C_4N_2H_{12}][U_2^{IV}F_6(HPO_3)_2]$, **2**, contains 11 non-hydrogen atoms, of which one uranium and one phosphorus atom are crystallographically independent (Supporting Information). Similar to **1**, the uranium atom is bonded to three oxygen and five fluorine atoms, adopting the distorted dodecahedral geometry (part a of Figure 2). The U−F bond distances are in the range of 2.178(4)−2.451(5) Å (average 2.335 Å), the shorter distance corresponding to the terminal U−F bond. The U−O bond distances are in the range of 2.266(6)−2.359(5) Å (average 2.32 Å). The O/F−U−O/F bond angles are in the range of 65.03(18)−144.74(19)°. The phosphorus atom has three P−O−U bonds. The P−O distances are in the range 1.521(6)−1.541(6) Å (average 1.530 Å.) The bond valence sum calculations indicate the valence state of uranium to be +4 ($\sum$s(U−O/F) = 3.87).[15] Selected bond distances are given in Table 2.

The basic polyhedral units, UO_3F_5 and HPO_3, in **2**, are similar to those observed in **1**, in addition to having the same secondary building unit, SBU-4 (part b of Figure 2). The SBU-4 units are connected through the fluorine bridges, forming an infinite 1D U−F−U chain structure (part a of Figure 2). Depending on the connectivity and arrangement of the atoms, two types of chains can be considered, which are interconnected through the oxygen atoms, forming the 3D structure (part b of Figure 2). This connectivity creates 8-membered 1D channels along the *a* axis, wherein the protonated piperazine molecules reside. The piperazine cations participate in hydrogen bond interactions of the type N−H···F and N−H···O, [N(1)−H(1)···F(1) (N−F = 2.668 Å, N(1)−H(1)···F(1) = 158°); N(1)−H(2)···O(2) (N−O = 2.856 Å, N(1)−H(2)···O(2) = 152°)].

$[C_4N_2H_{12}][(U^{VI}O_2)_2F_2(HPO_3)_2]$, 3. During the course of this study, we have also isolated a 2D compound, $[C_4N_2H_{12}][(U^{VI}O_2)_2F_2(HPO_3)_2]$, **3**, using 1-(2-aminoethyl) piperazine (AEPIP). The structure is formed by the networking of UO_5F_2 and HPO_3 units. The fluorine atoms bridge the uranium centers, forming a simple dimer, $[(UO_2)O_3]_2F_2$, which are connected through the corners by the HPO_3 units, forming the layered structure with 4- and 6-membered apertures (Figure 3). The protonated piperazine occupies the interlayer spaces. The AEPIP, which was used in the starting mixture, decomposed during the synthesis and gave rise to piperazine, and such behavior has been observed in many hydrothermal syntheses.[17] The bond valence sum calculations indicate the valence state of uranium to be +6 ($\sum$s(U−O/F) = 6.18).[15] The layer topology resembles the naturally occurring mineral johannite, $[Cu][(UO_2)_2(SO_4)_2(OH)_2]\cdot 8H_2O$.[18]

Discussion

The uranium phosphites **1**−**3** are members of a family of actinide inorganic framework compounds. The compounds, describe in this work, have been prepared under hydrothermal conditions by employing organic amines. In **1** and **2**, we observed the formation of compounds with U(IV), though the source of uranium (uranium acetate, U(VI)) was identical in all of the cases. Such reduction of the central metal ions has also been observed.[9a,9f] The unpredictable nature of the kinetically controlled solvent-mediated hydrothermal reactions is well illustrated by the formation of different phases of varying dimensionality and oxidation states of uranium.

Although all of the structures have bonding between the uranium center and the phosphite groups, they exhibit distinct differences. Whereas **1** and **3** are 2D, **2** has 3D connectivity. **1** and **3** appear to be the first members of 2D uranium phosphites. A careful examination of the structures of **1** and

(15) (a) Burns, P. C.; Ewing, R. C.; Hawthorne, F. C. *Can. Mineral.* **1997**, *35*, 1551. (b) Brese, N. E.; O'Keeffe, M. *Acta Crystallogr., Sect. B* **1991**, *47*, 192. (c) Broen, I. D.; Altermatt, D. *Acta Crystallogr., Sect. B* **1985**, *41*, 244.

(16) (a) Ferey, G. *Chem. Mater.* **2001**, *13*, 3084. (b) Ferey, G. *J. Solid State Chem.* **2000**, *152*, 37. (c) Ferey, G. *J. Fluorine Chem.* **1995**, *72*, 187. (d) Ferey, G.; Loiseau, T.; Lacorre, P.; Taulelle, F. *J. Solid State Chem.* **1993**, *105*, 179. (e) Ferey, G. *C. R. Acad. Sci. Paris, Ser. IIc* **1998**, *1*, 1. (f) Cavellec, M. R.; Riou, D.; Ferey, G. *Inorg. Chem. Acta* **1999**, *291*, 317.

(17) (a) Natarajan, S. *J. Mater. Chem.* **1998**, *8*, 2757. (b) Loiseau, T.; Ferey, G. *J. Fluorine Chem.* **2007**, *128*, 413, and the references therein.

(18) Mereite, K. *Tschermaks Mineral. Petrogr. Mitt.* **1982**, *30*, 49.

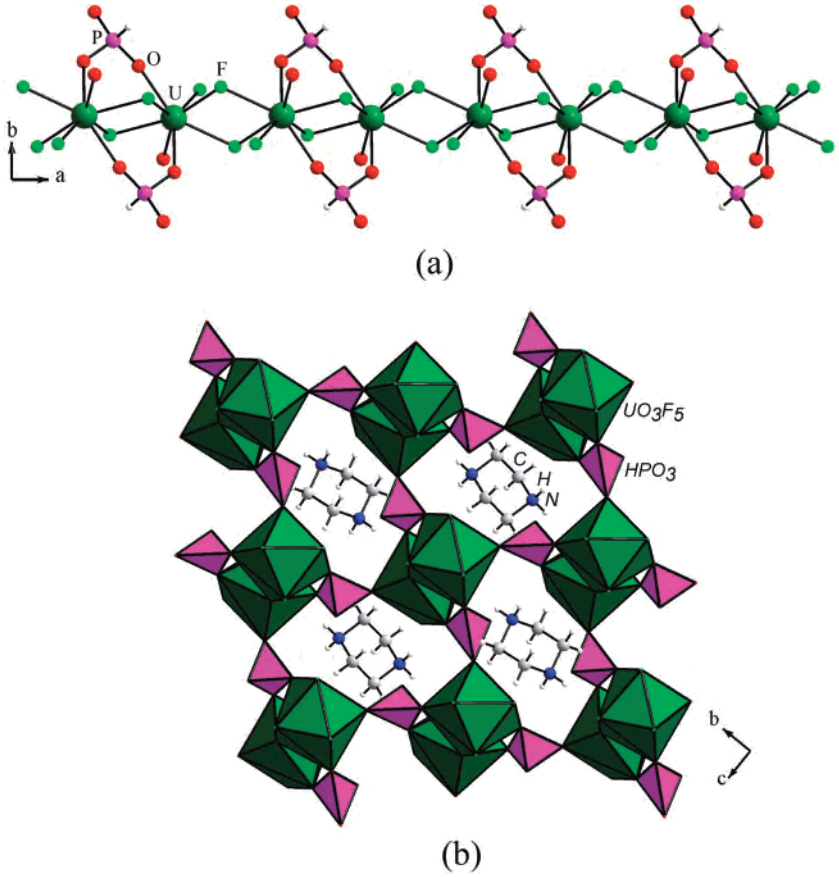

Figure 2. (a) 1D chains formed by the edge-shared connectivity between the SBU-4 units through the fluorine bridges in **2**. Note that identical chains are observed in the structure of **1**. (b) The polyhedral view of the structure of **2** in the *bc* plane showing the 1D channels with the piperazine molecule.

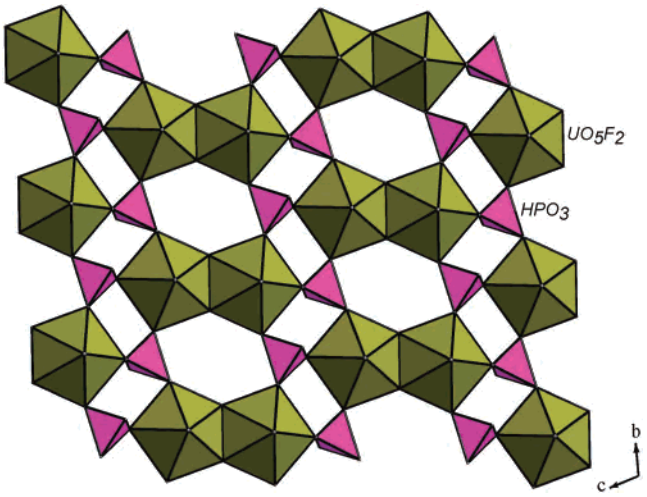

Figure 3. Polyhedral view of the uranium phosphite layer in $[C_4N_2H_{12}][(U^{VI}O_2)_2F_2(HPO_3)_2]$, **3**.

2 also reveals close relationships. In addition to having the same formula, and being formed by the same building unit, SBU-4, the connectivity involving the SBU-4 units creates the observed differences. In both the compounds, the SBU-4 units are connected through the fluorine bridges, forming the 1D chains. To the best of our knowledge, **1** and **2** appear to be the first examples of uranium phosphites formed exclusively by the SBU-4 unit. The formation of a 3D structure by SBU-4 units is noteworthy.

The structure of **2** can be compared and contrasted with the previously reported 3D uranium phosphite, $[C_4N_2H_{12}][(UO_2)_2(HPO_3)_2(H_2PO_3)_2]$.[8a] In $[C_4N_2H_{12}][(UO_2)_2(HPO_3)_2(H_2PO_3)_2]$, the uranium is in a +6 oxidation state, and the structure is formed by the connectivity between UO_7, HPO_3, and H_2PO_3 units, giving rise to 12- and 8-membered channels. In **2**, the uranium is in a +4 oxidation state, and the structure is formed by UO_3F_5 and HPO_3 units, giving rise to 8-membered channels.

Spectroscopic Studies. UV−vis absorption spectra were recorded in the solid state (Perkin-Elmer, lambda 35) at room temperature, which indicates the presence of U(IV) in **1** and **2** (part a of Figure 4). Both **1** and **2** exhibit comparable absorption bands. The observed bands and their assignments are $^3H_4 \rightarrow {}^3H_6$ (825 nm), $^3H_4 \rightarrow {}^1G_4$ (660 nm), $^3H_4 \rightarrow {}^1D_2$ (624 nm), $^3H_4 \rightarrow {}^3P_0$ (540 nm), $^3H_4 \rightarrow {}^3P_1$ (498 nm), $^3H_4 \rightarrow {}^1I_6$ (438 nm).

The photoluminescence spectra of all of the compounds were recorded at room temperature in the solid state. **1** and **2** show a strong emission band at ~366 nm, along with three weak bands at 402, 412, and 422 nm, when excited using a wavelength of 498 nm. The strong emission band corresponds to the $^1I_6 \rightarrow {}^3H_4$ transition, and the three weak bands correspond to the $^3P_2 \rightarrow {}^3H_4$ transitions (part b of Figure 4). The observation of emission bands at a lower wavelength compared to the excitation wavelength indicates a possible upconversion process in both of the compounds. Upconver-

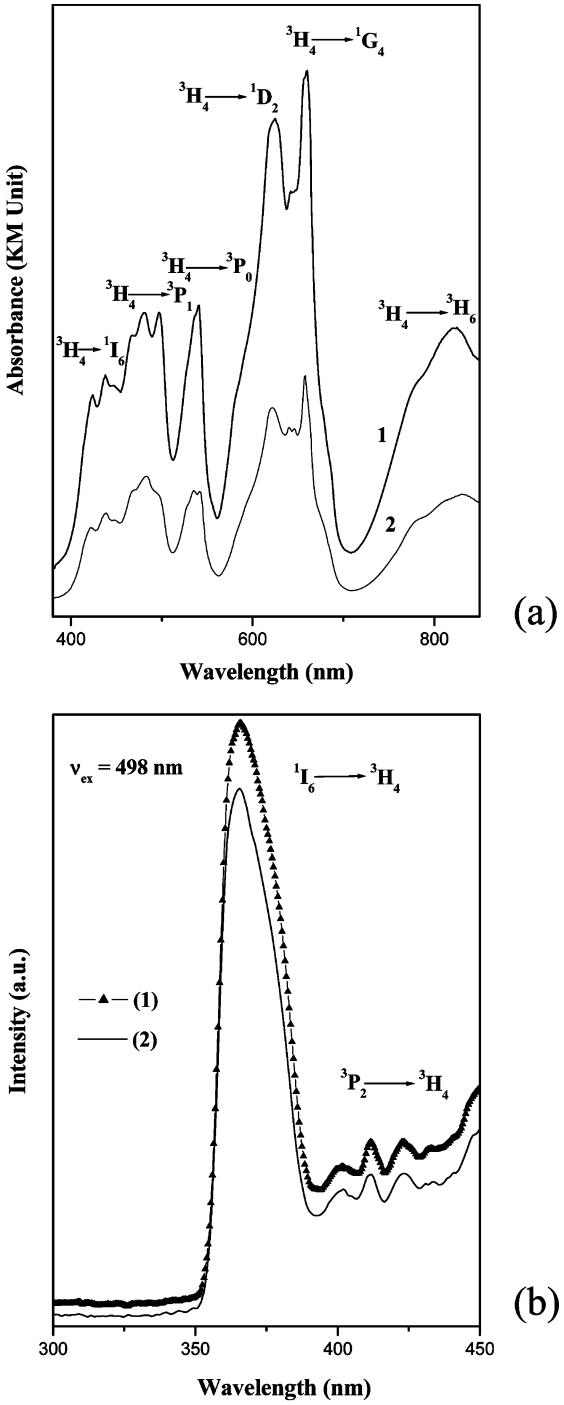

Figure 4. (a) Room-temperature UV−vis spectra of $[C_2N_2H_{10}][U_2^{IV}F_6(HPO_3)_2]$, **1,** and $[C_4N_2H_{12}][U_2^{IV}F_6(HPO_3)_2]$, **2**. (b) The room-temperature photoluminescence spectra of **1** and **2** (498 nm excitation). Note that the emission occurs at lower wavelengths through an upconversion process (text).

sion, generally observed in rare earth ions,[19] involves two-photon absorptions, and the emission is generally an anti-stokes one.[20] This may be useful for solid-state displays and detection of IR radiation in the visible region. It was proposed that the 5f electronic states of actinide ions in host crystals

Table 3. Data for Power Dependence Fluorescence Experiment

		emission intensity (I_{em})	
no. of slides	transmission intensity (I_{ex})	Compound **1**	Compound **2**
0	100	487.78	285.47
1	91.125	336.32	194.51
2	83.362	304.47	175.01
3	76.946	253.7	148.21
4	71.872	208.5	123.93
5	66.151	174.04	107.45
6	60.34	146.56	84.95

can be used for generating optical gain and upconversion emission.[21] Tetravalent actinide ions generally possess a larger crystal field splitting and spin−orbit coupling constant than those of the trivalent lanthanide ions, which could reduce the energy gap between the excited electronic states. This would lead to the observation of less fluroscence in actinide compounds.[22] Upconversion studies involving actinides have been carried out on doped compounds,[21a,21d] and to the best of our knowledge, there have been no reports of such investigations on open framework compounds containing U^{4+} ions.

The present studies indicate that in **1** and **2** the absorption process could be multiphotonic in nature. To understand the emission process and to correlate the dependency of the emission intensities with the excitation photon intensity, we have employed a simple relationship. According to this, if n numbers of photons are absorbed, then the emission can be related as,

$$I_{em} \propto (I_{ex})^n$$

or,

$$I_{em} = A(I_{ex})^n$$

or,

$$\log I_{em} = A1 + n \log I_{ex}$$

The value of n can be obtained from the log−log plot of I_{em} versus I_{ex}, where I_{em} is the emission intensity of any fluorescence peak, I_{ex} is the intensity of the excitation wavelength, and n is the order of the emission process, that is, the number of photons responsible for the emission. To perform these power dependence studies, we employed sterile glass slides sequentially, which varied the intensity of the incident beam. The transmission efficiency of the glass slides as a function of their number was precalibrated using the UV−vis spectrometer in the transmission mode and normalized with respect to a transmission obtained in the absence of any glass slides. The normalized transmission intensities (I_{ex}) as a function of the numbers of glass slides along with the corresponding fluorescence intensities (I_{em}) for the 366 nm peak is listed in Table 3 and shown in parts a and b of

(19) (a) Auzel, F. *Proc. IEEE* **1973**, *61*, 758. (b) Auzel, F. *Chem. Rev.* **2004**, *104*, 139.
(20) Blasse, G.; Grabmaier, B. C. *Luminescent Materials*; Springer-Verlag: New York, 1994.
(21) (a) Johnston, D.; Satten, R. A.; Wong, E. Y. *J. Chem. Phys.* **1965**, *44*, 687. (b) Krupa, J. C.; Carnall, W. T. *J. Chem. Phys.* **1993**, *99*, 8577. (c) Hubert, S.; Thouvenot, P. *J. Alloys Compd.* **1992**, *180*, 193. (d) Xu, W.; Dai, S.; Toth, L. M.; Peterson, J. R. *Chem. Phys.* **1995**, *193*, 339.
(22) Beitz, J. V.; Brundage, R. T. *J. Alloys Compd.* **1992**, *181*, 49.

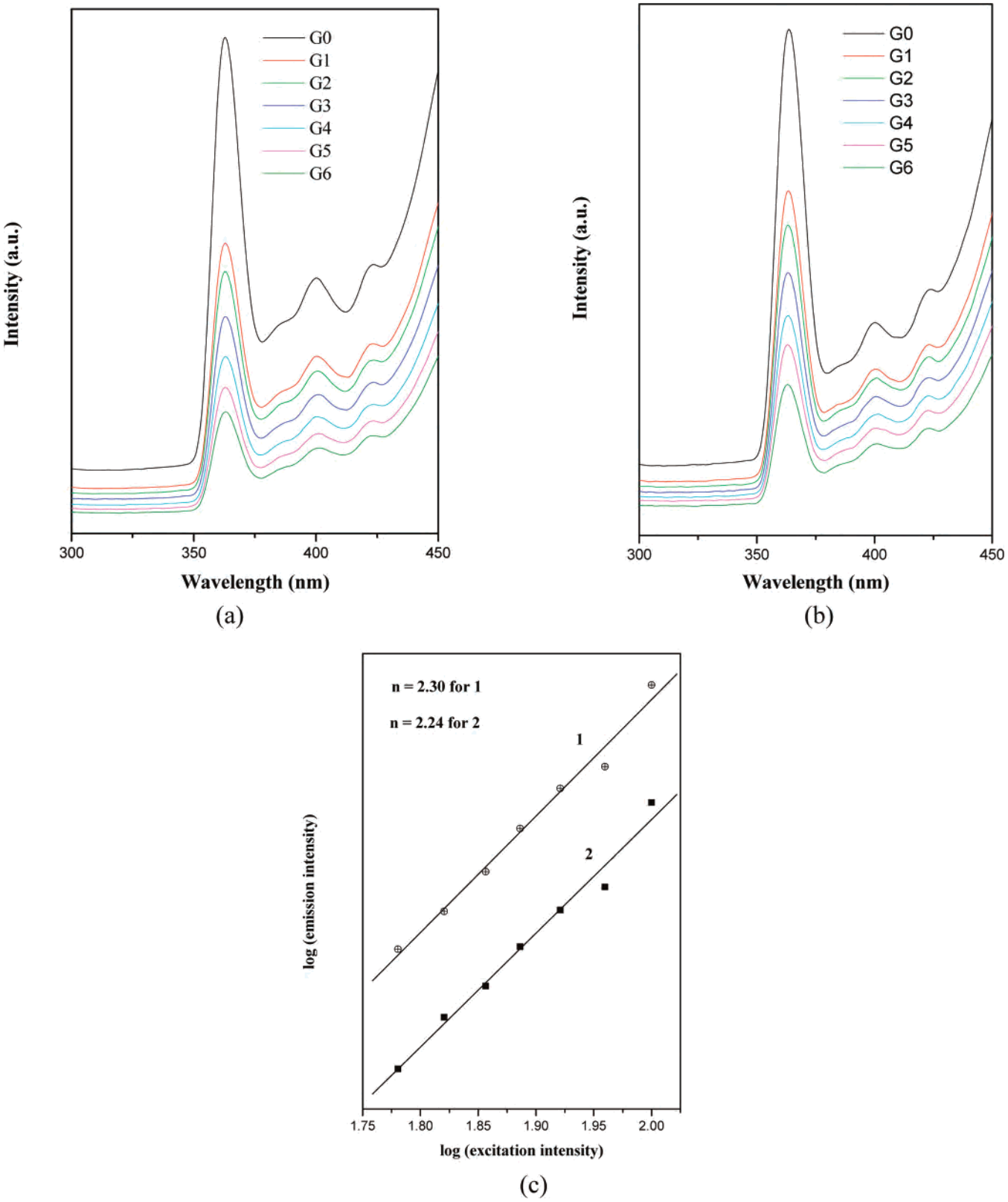

Figure 5. (a) Observed emission dependence on the excitation intensity of $[C_2N_2H_{10}][U_2^{IV}F_6(HPO_3)_2]$, **1**, (b) the observed emission dependence on the excitation intensity of $[C_4N_2H_{12}][U_2^{IV}F_6(HPO_3)_2]$, **2**. (c) The log−log plot of the excitation intensity dependence of the luminescence intensity for $\lambda = 498$ nm.

Figure 5. The log−log plot of the emission intensities as a function of the incident light intensities is shown in part c of Figure 5, which as expected was found to be linear, with slopes of 2.3 and 2.2 for **1** and **2**, respectively. This indicates that the upconversion behavior in **1** and **2** is preceded by the successive absorption of two photons.

The two-photon absorption, observed in **1** and **2**, can be rationalized by considering the schematic energy-level

Scheme 1. Schematic of the Free-Ion Energy Level Diagram for U^{4+} [a]

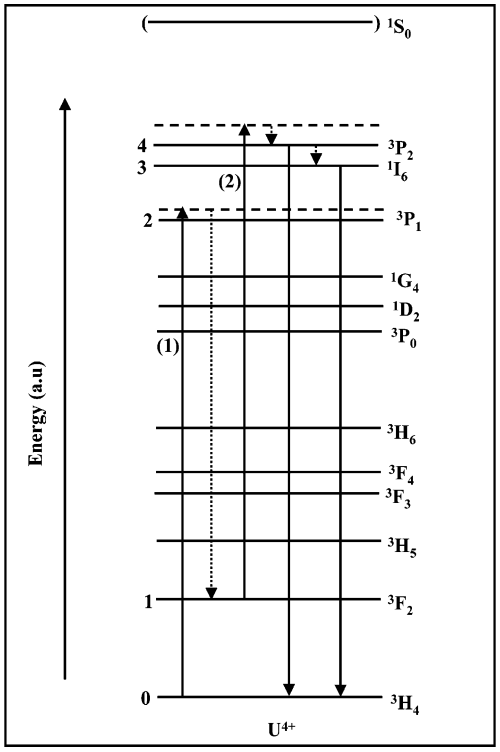

[a] Various possible excitation and emission pathways are indicated.

diagram for the U^{4+} ion (Scheme 1). As can be noted, absorption of the first photon excites the U^{4+} system from the ground state ($^3H_4$) to the excited $^3P_1$ state. The U^{4+} system can, then, nonradiatively decay to the $^3F_2$ state and absorb another 498 nm photon (if the lifetime of the $^3F_2$ state is long)[20d] and reach the $^3P_2$ and $^1I_6$ levels. Then, the upconverted emission in the observed region can result through the $^3P_2 \rightarrow {}^3H_4$ (366 nm) and $^1I_6 \rightarrow {}^3H_4$ (402, 412, and 422 nm) transitions.

Magnetic Studies. 1 and **2** have uranium in a +4 oxidation state and possess two unpaired electrons. We have carried out magnetic susceptibility studies of **1** and **2** on powdered samples in the temperature range 300−2 K using a SQUID magnetometer (MPMS, Quantum Design, USA). The temperature variation of the magnetic susceptibility is shown in part a of Figure 6. The magnetic susceptibility data follows the Curie−Weiss behavior in the temperature range 50−300 K, with $C = 1.12$ cm^3 K mol^{-1} and $\theta p = -59.82$ K for **1,** and $C = 1.22$ cm^3 K mol^{-1} and $\theta p = -64.10$ K for **2**. For both of the compounds, μ_{eff} decreases with decreasing temperature (part b of Figure 6). The negative θp value and the decrease of μ_{eff} with temperature indicate the presence of antiferromagnetic interactions. The effective net magnetic moment per uranium at 300 K is 2.75 μ_B for **1** and 2.85 μ_B for **2**, which are in agreement with the values observed in other U^{4+} compounds (2.7−3.6 μ_B).[9b,9d,9k,9m] The effective moment decreases rapidly below ~50 K with decreasing temperature (part b of Figure 6), suggesting the presence of antiferromagnetic interactions. It is likely that the presence of a zero-filed splitting for the $5f^2$ ion (U^{4+}) and a nonmagnetic ground state may contribute to the change in the magnetic moment. The magnetic susceptibility data of **2** exhibits a different behavior compared to **1**, especially at low temperatures. The susceptibility of **2** appears to be leveling off below 15 K to 0.012 emu/U(IV) ion, indicative

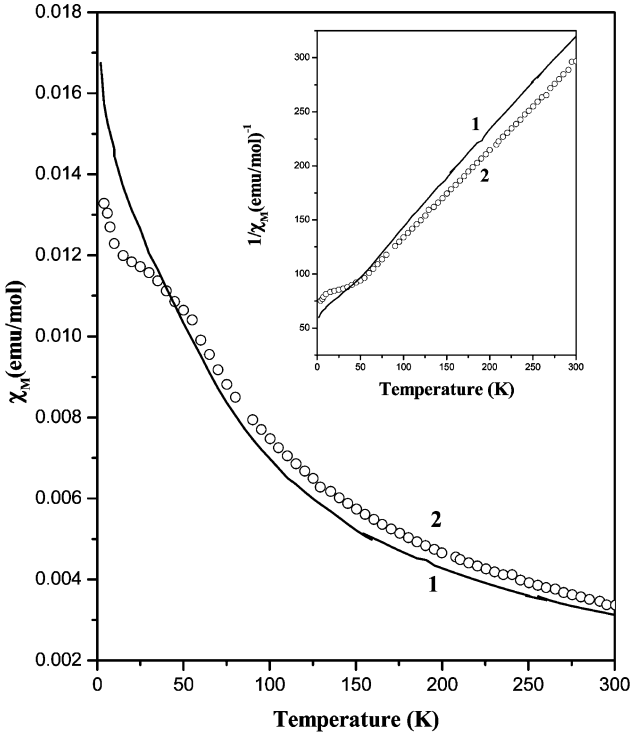

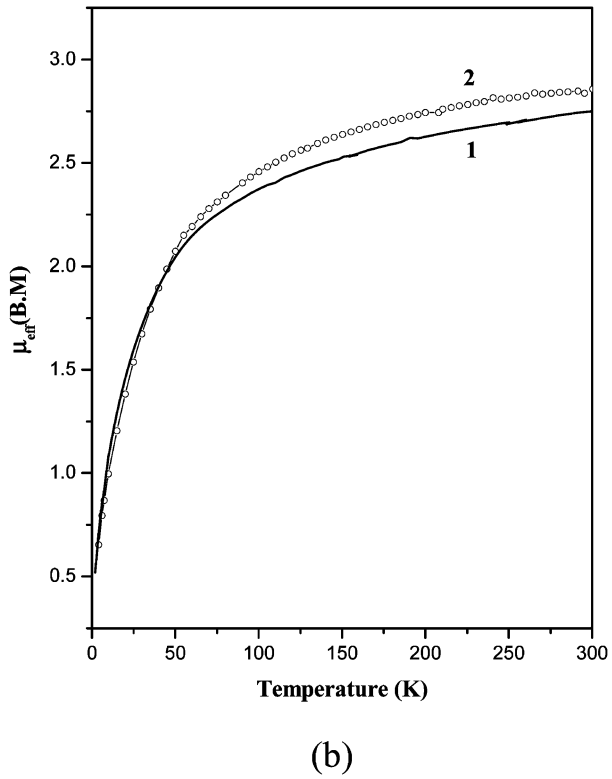

Figure 6. (a) Thermal variation of the magnetic susceptibility for **1** and **2**. The inset shows the variation of the inverse magnetic susceptibility with temperature. (b) The μ_{eff} versus T plot for the **1** and **2**.

of a possible nonmagnetic ground state.[9a,9f,9n,23] In addition, the 3D nature of the structure of **2** also contributes to the complexity of the magnetic interactions between the U^{4+} ions. The magnetic interactions of the U^{4+} compounds **1** and **2** appear to be complex and would require detailed theoretical modeling for better understanding.

Conclusion

Three new uranium phosphites, $[C_2N_2H_{10}][U_2^{IV}F_6(HPO_3)_2]$, **1**, $[C_4N_2H_{12}][U_2^{IV}F_6(HPO_3)_2]$, **2**, and $[C_4N_2H_{12}][(U^{VI}O_2)_2F_2(HPO_3)_2]$, **3**, have been synthesized hydrothermally in the presence of structure-directing organic amines. The structures consist of $U(O/F)_x$ ($x = 7$, 8) and HPO_3 polyhedral units linked together forming two- (**1** and **3**) and three-dimensionally (**2**) extended structures. The formation of SBU-4 units and infinite U−F−U chains in **1** and **2** is noteworthy. To the best of our knowledge, simple secondary building units (SBU-4) have been observed for the first time in actinide-based framework compounds. We have also been able to show that the upconversion behavior observed in U^{4+} compounds (**1** and **2**) is a two-photon process, and the emission is in the blue region. The magnetic studies indicate antiferromagnetic behavior in **1** and **2**.

Acknowledgment. The authors thank Professor P. K. Das of Inorganic and Physical Chemistry Department, Indian Institute of Science, Bangalore, India, for many helpful suggestions. The authors also thank the reviewers for their many helpful suggestions. S.N. gratefully acknowledges the Department of Science and Technology (DST), Government of India, for the award of a research grant and also for the award of a RAMANNA Fellowship. The authors thank DST-IRHPA (India) for the CCD facility. M.C. thanks the Council of Scientific and Industrial Research, Government of India, for the award of a research fellowship.

Supporting Information Available: X-ray crystallographic files in CIF format, bond distances and bond angles, powder X-ray diffraction patterns, IR, and TGA curves for all of the compounds. This material is available free of charge via the Internet at http://pubs.acs.org.

IC700866F

(23) (a) Santini, P.; Lémanski, R.; Erdös, P. *Adv. Phys*. **1999**, *48*, 537. (b) Erdös, P.; Robinson, J. M. *The Physics of Actinide Compounds*; Plenum Publishing: New York, 1983.